Spiking in a semiconductor device: Experiments and comparison with a model

F.-J. Niedernostheide

Institut für Angewandte Physik, Universität Münster, Corrensstraße 2/4, D-48149 Münster, Germany

H.-J. Schulze

Siemens AG, Otto-Hahn-Ring 6, D-81730 München, Germany

S. Bose, A. Wacker,[*] and E. Schöll

Institut für Theoretische Physik, Technische Universität Berlin, Hardenbergstaße 36, D-10623 Berlin, Germany

Silicon p^+-n^+-p-n^- devices exhibit periodic and nonperiodic self-organized current oscillations. It is shown that the oscillations are caused either by spatiotemporal spiking of a current filament which decays immediately after its generation or by homogeneous relaxation oscillations of the current density. Moreover, the experiments give clear evidence for complex spatiotemporal spiking, i.e., a filament emerges and vanishes in an irregular temporal sequence. A comparison with a simple model reveals good qualitative agreement with the observed bifurcation scenarios. [S1063-651X(96)12008-0]

I. INTRODUCTION

A variety of mechanisms involving an autocatalytic (activating) process and an inhibiting feedback enable the self-organized appearance of localized structures, e.g., in the form of current-density filaments in semiconductors or semiconductor devices. Very often the formation of a localized structure is accompanied by self-sustained oscillations of the current or the voltage due to the generation and subsequent extinction of the localized structure.

In experiment, spiking current filaments have been observed, e.g., in silicon [1] and GaAs [2] p-i-n diodes and in silicon p-n-p-n devices [3]. There is also experimental evidence for similar behavior in n-GaAs and p-Ge [4,5]. Spiking behavior has also been observed in electron-hole plasmas [6]. In a semiconductor gas-discharge system filaments switching on and off and moving in an irregular manner have been observed experimentally and described in terms of a two-layer model [7]. The properties of spiking localized structures have been studied in detail in Refs. [8,9] by analyzing reaction-diffusion systems. Recently, a specific model for the heterostructure hot-electron diode has been derived [10,11] and used to propose a simple generic model which shows spiking independently of the particular conduction mechanism involved [12]. Detailed bifurcation scenarios have been predicted from this model [13].

However, investigations about bifurcation scenarios of spiking filaments in semiconductors that allow a comparison between experimental and theoretical results of both integral quantities and the local dynamics are rare. An important reason for this is the fact that spiking filaments typically bifurcate from a low current-density state; this makes a spatiotemporally resolved characterization of the basic state more difficult in the experiment. Moreover, even the direct measurement of a spiking filament often is difficult. Conse-

quently, most of the previous works dealing with spiking filaments in semiconductors consider only integral quantities and in the few cases where extended spatiotemporally resolved measurements have been performed (see, e.g., Ref. [1]), a comparison with theoretical results has not been performed.

In this paper we therefore study the spiking behavior of current-density filaments in silicon p^+-n^+-p-n^- diodes and draw a comparison with the predictions following from the reaction-diffusion model [12,13]. The main bifurcation parameters are the external dc driving voltage V_s and a capacitance C connected parallel to the sample and determining the temporal evolution of the device voltage. By means of spatially and temporally resolved measurements of the recombination radiation we show that there is a strong correlation between the *global* current and voltage oscillations and the *local* dynamics of the current-density distribution in the form of spiking filaments. This makes it possible to provide a systematic analysis of the spatiotemporal behavior of the current density as function of the two parameters V_s and C.

II. EXPERIMENTAL RESULTS

The p^+-n^+-p-n^- devices are prepared by a combination of conventional diffusion technique and ion implantation. In order to provide nonblocking electrical contacts to the high-resistivity n^- substrate an additional n^+ layer has been implanted. Finally, aluminum has been evaporated on both wafer sides. The wafers have been diced into samples with contact areas of typically 5×1 mm^2. Details of the preparation can be found in Ref. [3].

The device is connected to a dc voltage source V_s via a load resistor R_0 in such a way that the p^+ layer is positively biased with respect to the n^- layer. Thus, the middle n^+-p junction is reverse-biased and causes a low-current branch in the current-voltage characteristic $I(V)$ (Fig. 1). When the device voltage reaches values of ≈ 50 V, the electric field in the space charge region of the n^+-p junction is sufficiently

---

[*]Present address: Microelectronic Centre, Technical University of Denmark, DK-2800 Lyngby, Denmark.
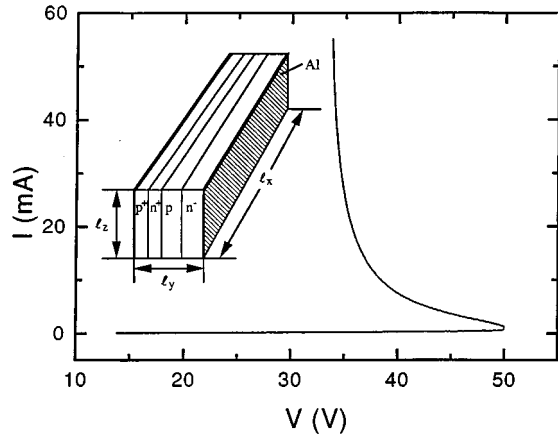
FIG. 1. Measured stationary current-voltage characteristic $I(V)$ of a p^+-n^+-p-n^- diode; $R_0 = 20$ kΩ. The inset shows the typical geometry of a diode. All experimental results presented in this work belong to a sample with $l_x = 3.6$ mm, $l_y = 0.87$ mm, $l_z = 0.84$ mm.

FIG. 2. Amplitude V_{ss} and frequency f of the ac part of the time trace $V(t)$ as a function of the driving voltage V_s near the critical voltage $V_{s,c1} = 73.2$ V for $R_0 = 20$ kΩ, $C = 0.02$ μF.

large so that impact ionization takes place leading to an autocatalytic increase of charge carriers. The charge carriers are immediately separated in the high-field zone and cause an additional carrier injection when they reach the outer p-n junctions. This leads to the regime of negative differential resistance in the $I(V)$ characteristic as shown in Fig. 1. For sufficiently large currents, the differential resistance becomes positive again leading to an S-shaped $I(V)$ characteristic. From measurements presented in earlier work [3,14] it is known that the current-density distribution in the low-current branch of the $I(V)$ characteristic is uniform; when proceeding along the branch with negative differential resistance upon increasing current, the current-density distribution contracts to a current-density filament. The contraction phase is typically completed for current values of ≈ 20 mA; then a filament with a well-defined width is stable.

The system behavior changes drastically when a sufficiently large capacitance ($C \gtrsim 5$ nF) is connected parallel to the device. In this case we observe spontaneously arising oscillations of the device current and the device voltage. A typical scenario for increasing the voltage V_s can be described as follows: When V_s exceeds a critical value $V_{s,c1}$, small-amplitude oscillations appear with a frequency f of about 4.3 kHz at $V_{s,c1}$ (Fig. 2). The amplitude of the oscillations rises continuously from zero with increasing V_s (Fig. 2) indicating a supercritical Hopf bifurcation. At a second critical value $V_{s,c2}$ large-amplitude oscillations superimpose on the small-amplitude oscillations. These oscillations vanish when the voltage V_s exceeds a third critical value $V_{s,c3}$. When the voltage is decreased from large values, the large-amplitude oscillations appear at a value $V_{s,c4} < V_{s,c3}$. Thus, there is a hysteretic behavior indicating a subcritical bifurcation. When the voltage is further decreased at $V_{s,c2}$ the small-amplitude oscillations appear instead of the large-amplitude oscillations and at $V_{s,c1}$ the oscillations vanish completely. Note that within experimental error no hints for hysteretic behavior have been found for either the transition at $V_{s,c2}$ or that at $V_{s,c1}$.

In order to get insight into the spatiotemporal behavior of the current-density distribution, the recombination radiation
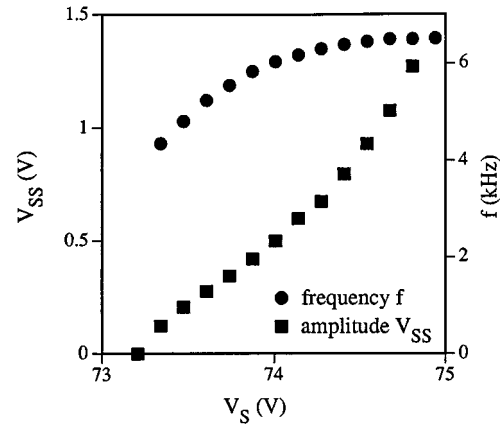
was measured by using a gated high-sensitivity near-infrared video camera (Hamamatsu Model No. C2741) with minimal gate times down to 10 ns. In all measurements presented in this work one of the x-y planes of the sample (cf. Fig. 1) was focused to the $S1$ photocathode of the camera. As the recombination radiation of silicon is rather weak, it is necessary to integrate about several hundreds to thousands of single shots. For that purpose the self-sustained voltage oscillations have been used to generate a trigger pulse the delay and width of which could be adjusted in such a way that it was possible to image the radiation distribution at any stage of the period with a suitable gate time.

In Figs. 3(a)–3(c) time traces of the device voltage $V(t)$, the sample current $I(t)$, and the I-V phase portrait are depicted for a typical small-amplitude oscillation. Figures 3(d) and 3(e) show the measured distribution of the recombination radiation at two different times. They correspond to the times at which the current trace reaches its maximum and minimum, respectively. The white lines mark the imaged $l_x \times l_y$ area of the sample. The main current flow direction is from the right to the left. On the top of Fig. 3(d) the sequence of the multilayered structure is indicated schematically. In both camera records the light intensity is distributed uniformly. However, in Fig. 3(e) the light intensity is located mainly near the anode while in Fig. 3(d) also a nearly uniform emission near the cathode can be recognized and the light intensity near the anode is greater than in Fig. 3(e). Thus, we may conclude that the light intensity distribution performs a homogeneous relaxation oscillation. Taking the light intensity distribution as a first approximation for the current-density distribution this in turn implies that the small-amplitude oscillations are connected with homogeneous oscillations of the current density.

Figure 4 elucidates the case of large-amplitude oscillations. While $V(t)$ changes still quite slowly in the course of time [Fig. 4(a)], the sample current $I(t)$ [Fig. 4(b)] shows sharp peaks with a width of about 5 μs. The I-V phase portrait [Fig. 4(c)] reveals that the oscillation covers a large area in this place and, in particular, encloses nearly completely the branch with the negative differential resistance of the stationary $I(V)$ characteristic (cf. Fig. 1). The camera
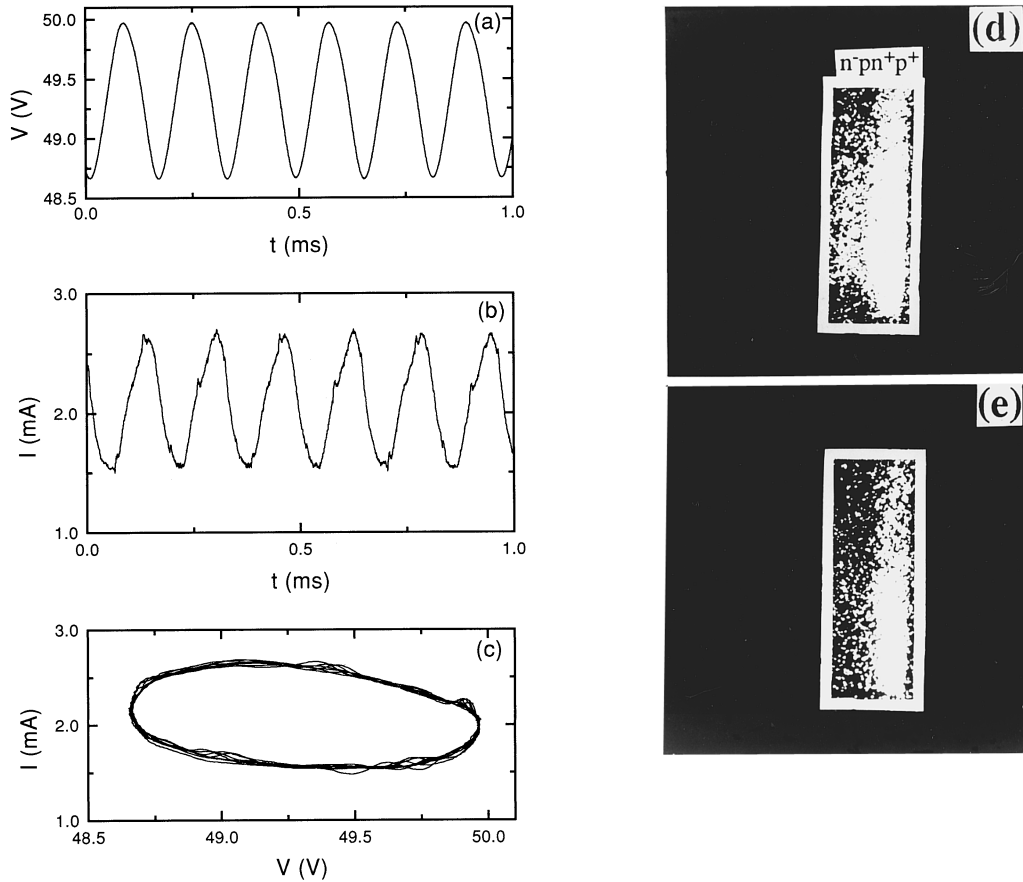
FIG. 3. Time trace of the device voltage $V(t)$ (a), the sample current $I(t)$ (b), and corresponding phase portrait of I versus V (c); the camera records show the emitted light intensity distribution in the maximum (d) and minimum (e) of $I(t)$, indicating a homogeneous relaxation oscillation. Parameters: $R_0 = 10$ kΩ, $C = 0.02$ μF, gate time $= 10$ μs, number of integrated single shots $= 33\,167$.

records depicted in Figs. 4(d)–4(f) indicate that the peak appearing in the time trace $I(t)$ is caused by a spiking filament. Figure 4(d) shows the light intensity distribution when the sample current is maximal. Apparently, a localized current filament has been formed. The strong current through the filament causes a rapid partial discharge of the capacitance C. The record shown in Fig. 4(e) has been taken 10 μs after the current peak. The filament is still observable; however, the light intensity is drastically reduced in comparison to Fig. 4(d) indicating that the filament fades away. 60 μs after the generation the filament is completely extinguished [Fig. 4(f)]. It rises again with the next current peak. When the number of integrated single shots is increased, we find that during the low-current phases, in which no filament is present, a weak uniform light intensity distribution is observable, indicating a uniform low current-density state. Thus, these data imply that the periodic large-amplitude oscillations emanate from a periodically spiking filament that fades away immediately after it has been nucleated; during the recovery time the current density relaxes to a uniform state from which a new spiking filament is generated in the next cycle.

By using the results that the small-amplitude and large-amplitude oscillations correspond to homogeneous relaxation oscillations and spiking filaments, respectively, we are now able to provide a systematic classification of the spatiotemporal behavior of the current density connected with these

oscillations in the device under consideration. For that purpose, the C-V_s control parameter space was scanned by a stepwise increase of the voltage V_s starting from a value corresponding to a uniform current-density distribution up to a value at which a static filament is stable. Subsequently, the voltage was decreased to the original value in order to measure hysteresis loops. This procedure was repeated for various capacitances. In Fig. 5 the bifurcation points, determined by evaluating time series of the sample current as described above, are marked by different symbols in the C-V_s control parameter space. The lines are introduced to guide the eye and to separate the regions in which different behavior has been observed. Clearly, we can distinguish five different regions: For low values of V_s the system realizes stable uniform current-density distributions which become unstable in favor of uniform relaxation oscillations or a spiking filament when V_s exceeds $V_{s,c1}$. The former ones are stable only in a small voltage interval and transform also to spiking filaments at $V_s = V_{s,c2}$. Periodically spiking filaments can be stabilized in a wide parameter range. In the region that is bounded by the lines through the triangles and the rhombi, bistability of spiking and static filaments has been found. For even larger voltages only the latter are stable. Note that the width of the bistable region where a static and a spiking filament can be stabilized at the same value of V_s decreases with increasing C.
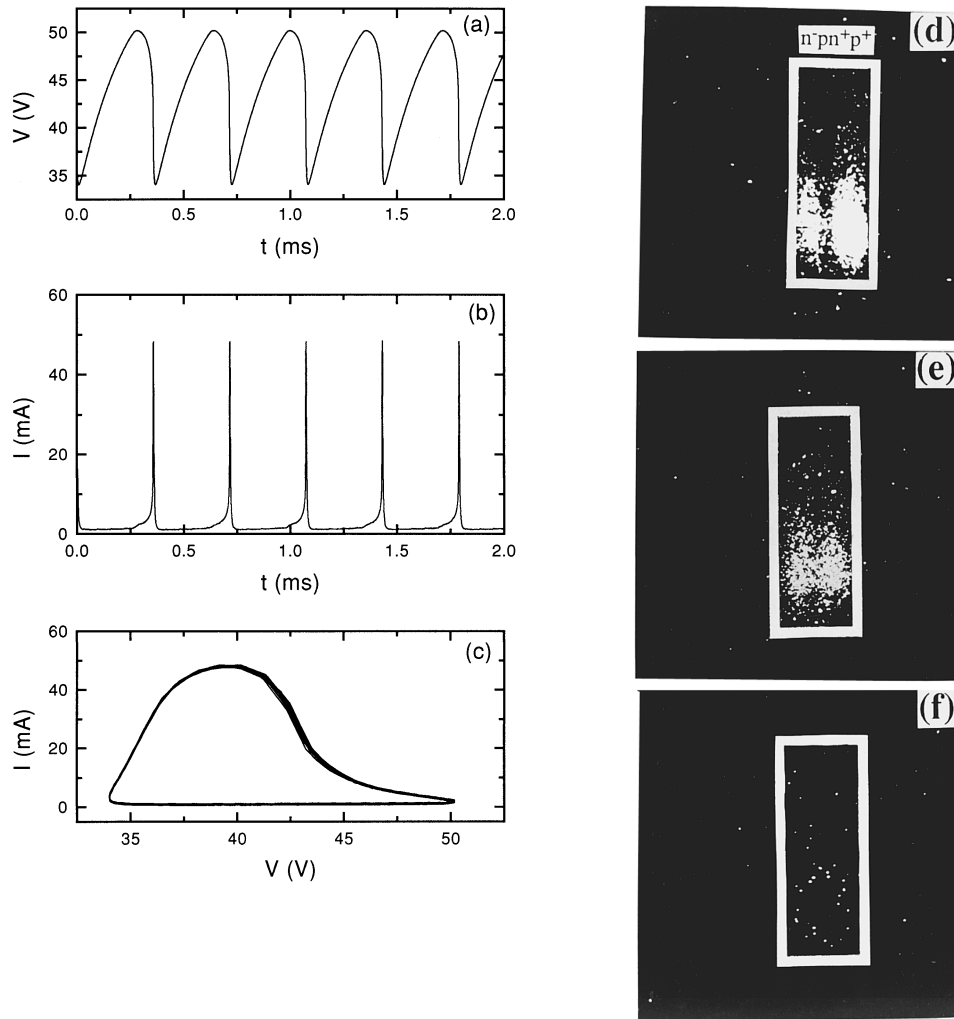
FIG. 4. Time trace of the device voltage $V(t)$ (a), the sample current $I(t)$ (b), and corresponding phase portrait of I versus V (c); the camera records show the emitted light intensity distribution in the maximum (d) of $I(t)$ and with a delay of 10 μs (e) and 60 μs (f) with respect to (d) and indicate a spiking filament. Parameters: $R_0 = 20$ kΩ, $C = 0.02$ μF, gate time $= 1$ μs, number of integrated single shots $= 27\,850$.

The transition from the homogeneous relaxation oscillation to the periodically spiking filament takes place in a very small voltage interval. A detailed analysis of the time traces $I(t)$ at this transition reveals that the transition consists of two stages: At voltage values just below the appearance of spikes the amplitude of the homogeneous oscillations shows small fluctuations, indicating that the spatially uniform oscillation becomes temporally irregular. With increasing voltage V_s the amplitude fluctuations of the small-amplitude oscillations increase and the onset of the spiking regime is characterized by an occasional appearance of large-amplitude current spikes in an irregular manner as shown in the time trace of $I(t)$ in Fig. 6. The duration of the phases in which the current density oscillates homogeneously varies statistically. With increasing V_s, the mean duration of these phases decreases and, finally, a periodic signal develops. The strong correlation between the appearance of the peaks of $I(t)$ and the nucleation of a spiking filament in the case of periodic large-amplitude oscillations suggests that the peaks appearing irregularly in $I(t)$ are connected with complex nonperiodic spatiotemporal spiking of a filament.

III. MODEL EQUATIONS AND COMPARISON WITH EXPERIMENTS

In Ref. [12] a simple noncubic reaction-diffusion model has been proposed for investigating the properties of spiking which we will call generic model in the following. The model equations in dimensionless units are

$$\frac{\partial a(x,t)}{\partial t} = f(a(x,t),u(t)) + \frac{\partial^2 a(x,t)}{\partial x^2}, \quad (1)$$

$$\frac{du(t)}{dt} = \alpha \left(j_0 - \frac{1}{l_x} \int_0^{l_x} dx\, j(a(x,t),u(t)) \right) \equiv \alpha(j_0 - \langle j \rangle), \quad (2)$$

with the functions

$$f(a,u) = \frac{u-a}{(u-a)^2 + 1} - Ta, \quad (3)$$

$$j(a,u) = u - a. \quad (4)$$
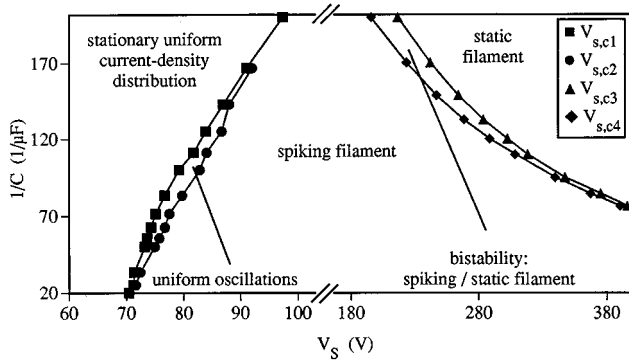
FIG. 5. Classification of the observed spatiotemporal behavior in the C-V_s control parameter space for $R_0 = 20$ kΩ. The symbols mark experimentally determined bifurcation points from uniform current-density distributions to uniform oscillations or spiking filaments (squares), from uniform oscillations to spiking filaments (circles), and from spiking to static filaments (triangles) or vice versa (rhombi).

The variables $u(t)$ and $a(x,t)$ represent the sample voltage and the internal degree of freedom responsible for bistability, respectively. In terms of the underlying nonlinear dynamics a and u correspond to an activator and an inhibitor variable, respectively. The control parameter j_0 is proportional to the external current assuming current controlled conditions which are appropriate for the large load resistance used in the experiment. l_x denotes the width of the sample where we use Neumann boundary conditions for $a(x,t)$ at $x=0$, l_x (see inset of Fig. 1). T parametrizes the local S-shaped steady-state current-voltage characteristic. The parameter α is approximately given by the ratio C_2/C, where C is the external capacitance, and C_2 is the capacitance of the layer whose conductivity essentially changes during the switching process [12]. For the given system, we approximate C_2 by the capacitance of the n^+-p junction which is of the order of ≈ 2 nF for a voltage of 30 V across this junction. With the experimental values of $C = 0.02$ μF we therefore find values of α of the order of 0.1. Indeed we obtain spiking in the generic model for values of $0.01 < \alpha < 0.1$, approximately.

A linear stability analysis shows that the homogeneous steady state becomes unstable against homogeneous fluctuations if

$$\alpha < \frac{j_0^2 - 1}{(1+j_0^2)^2} - T. \qquad (5)$$

At equality we find a supercritical Hopf bifurcation which generates homogeneous limit cycle oscillations. Inhomogeneous fluctuations of the form $\delta a(x,t) \sim \cos(\pi x/l_x)e^{\lambda t}$ grow exponentially in time for

$$\frac{\pi^2}{l_x^2} < \frac{j_0^2 - 1}{(1+j_0^2)^2} - T. \qquad (6)$$

As shown in Refs. [12,13], this system exhibits the following types of stable states depending on the parameters α: stationary homogeneous, oscillatory homogeneous (Fig. 7), stationary filamentary, periodically spiking (Fig. 8), and chaotically spiking. The spiking state is characterized by the
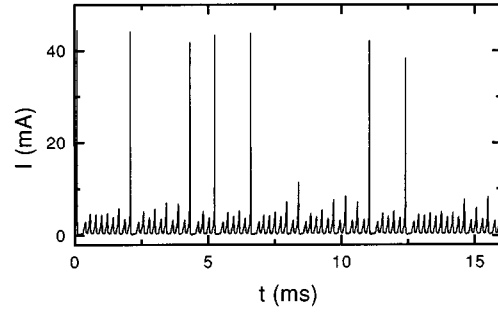
FIG. 6. Nonperiodic time trace $I(t)$ near the transition from a homogeneous relaxation oscillation to a periodically spiking filament. Parameters: $R_0 = 20$ kΩ, $C = 0.02$ μF, $V_s = 76.75$ V.

formation of an inhomogeneous current-density distribution $j(x,t)$ which decays immediately afterwards. The time interval between the spikes is sensitively determined by the time the trajectory in phase space remains close to the unstable homogeneous state. As the inhomogeneity is usually very small after the spike has vanished, this time interval may be quite large, especially close to the onset of spiking, where the homogeneous state becomes unstable against spatial fluctuations.

For $T = 0.05$ and $l_x = 40$ we have investigated the dynamical behavior by a numerical integration of the differential equations (1) and (2) for a large amount of different parameters j_0 and α. The individual behavior after transients died out is marked by specific symbols in the j_0-α control parameter space as presented in Fig. 9. One can easily distinguish specific regions where stable filaments, periodic spiking, chaotic spiking, and homogeneous oscillations occur. Additionally, we have depicted the lines resulting from the stability analysis. Line 1 in Fig. 9 marks the supercritical Hopf bifurcation given by Eq. (5) and line 2 denotes the instability against inhomogeneous fluctuations given by Eq. (6).

Originally, the generic model (1),(2) was proposed as a general mechanism for spatiotemporal spiking [12] independently of the p-n-p-n structure considered here. Therefore the functions $f(a,u)$ and $j(a,u)$ are not connected to the specific physical transport mechanisms. Now we will investigate in how far this generic model describes the same qualitative features as seen in the experiment.

At first we note that the type of homogeneous oscillations (Fig. 7) is in good qualitative agreement with the experimental data (Fig. 3). The spiking behavior as depicted in Fig. 8 exhibits a spatiotemporal current-density distribution which is in qualitative agreement with the behavior of the observed recombination radiation in Fig. 4 if we assume that the intensity of the radiation is related to the local current density.

Nevertheless, the temporal behavior of both the current and the voltage in the case of spiking are different with respect to the following points: The shape of the oscillations is different from that observed in experiment, where the current exhibits extremely sharp peaks, while the voltage changes more smoothly. We think that these differences may be caused by the detailed form of the functions $f(a,u)$ and $j(a,u)$. Second, the theoretical results exhibit long phases between the spikes where both $\langle j \rangle$ and u are almost constant. During these phases the phase trajectory is very close to the
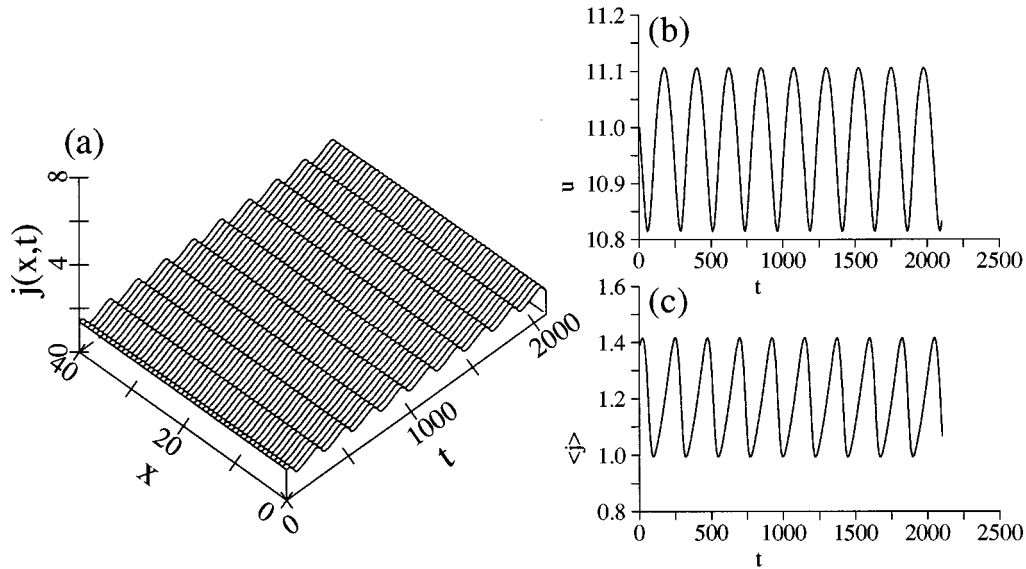
FIG. 7. Calculated current density $j(x,t)$ as a function of space x and time t (a), voltage time signal $u(t)$ (b), and sample current time signal $\langle j \rangle$ (t) (c) of the homogeneous oscillations ($\alpha = 0.02$, $j_0 = 1.2$, dimensionless units).

homogeneous fixed point of the model equation, so that the growth of the inhomogeneity takes a long time. This growth process is extremely sensitive to noise or spatial inhomogeneities inside the sample since these destroy the homogeneity of the fixed point. In order to check these two assumptions we have performed simulations with a spatially varying $T(x) = T_0 + \Theta(x - l_x/2)\delta T - \Theta(l_x/2 - x)\delta T$. Using $T_0 = 0.02$, $\delta T = 10^{-4}T_0$, we obtain the temporal behavior depicted in Fig. 10, which is in much better agreement with the experimentally observed behavior. [A similar result is obtained by adding spatiotemporal noise to the model equation instead of introducing a spatially dependent $T(x)$.]

Now we compare the bifurcation scenarios of the generic model (Fig. 9) and the experiment (Fig. 5). Here we have to identify $\alpha \sim 1/C$ and $j_0 \sim V_s$. The experimentally observed transition from the spiking to the static filamentary state with increasing bias V_s (right hand side of Fig. 5) is in good agreement with the simulation of the generic model. In both cases a certain range of bistability between both states is found. Our theory [13] predicts that the static filament becomes unstable via a subcritical Hopf bifurcation. In the experiment we find a spiraling out of the $j(t)$ signal from the old fixed point on decreasing the voltage over $V_{s,c4}$, which is in good agreement with a subcritical Hopf bifurcation.

The left-hand side of the experimental bifurcation diagram (Fig. 5) shows that the spiking behavior is generated
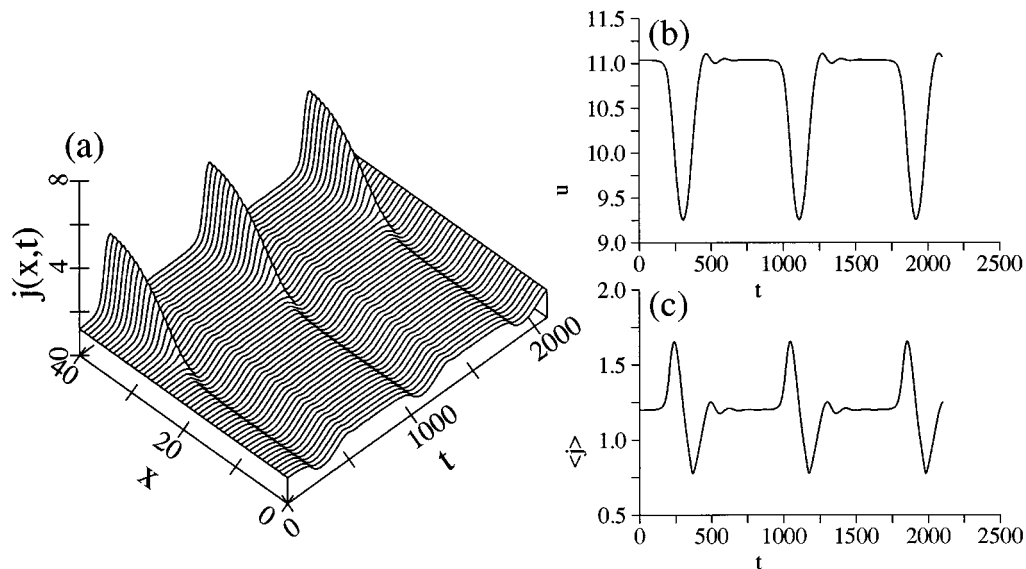
FIG. 8. Calculated current density $j(x,t)$ (a), voltage time signal $u(t)$ (b), and sample current time signal $\langle j \rangle(t)$ (c) of the periodic spiking ($\alpha = 0.05$, $j_0 = 1.2$).
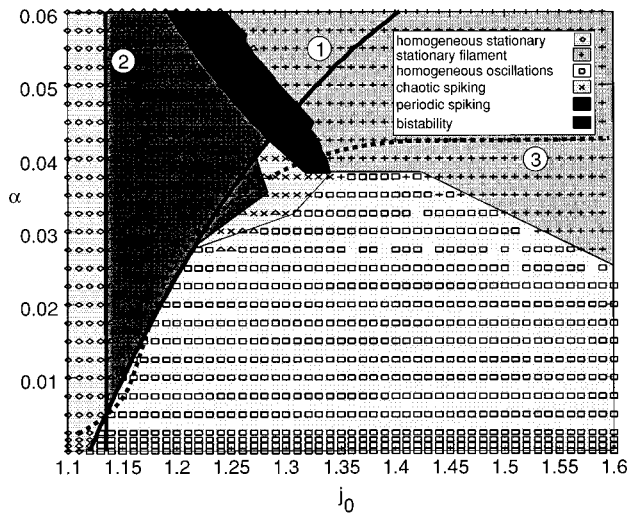
FIG. 9. Calculated phase diagram of the control parameters α, j_0. Line 1 is the result of a linear stability analysis [see Eq. (5)] and marks the points where the homogeneous steady state becomes unstable against homogeneous fluctuations. Line 2 denotes the points where the homogeneous state becomes unstable against inhomogeneous fluctuations [see Eq. (6)]. The dotted line (3) marks a possible path through the bifurcation diagram exhibiting the same bifurcation scenario as found experimentally.

from the homogeneous steady state via a small regime of homogeneous oscillations which occur for a lower bias. This is in contrast to the result from the generic model where the spiking behavior is generated directly from the stationary homogeneous steady state, which becomes unstable against pattern formation. We suggest that this difference may be related to the following two aspects.

One important aspect could be the fact that the internal capacitance C_2 of the device is not a fixed quantity but strongly depends on the voltage and the state in which the

diode is operated. As soon as the autocatalytic process becomes effective the sample current is strongly increasing and causes changes in the voltage drops across the p-n junctions, leading to an increase of the junction capacitances. As the mean sample current increases with increasing V_s, the capacitance C_2 should effectively increase with increasing V_s. With fixed external capacitance C the quantity $\alpha \approx C_2 / C$ should then increase with the external current j_0. This means that the path through the bifurcation diagram might not be a horizontal line at fixed α with increasing j_0 but a more complicated curve as indicated by the dotted line in Fig. 9. Following this line we successively find a homogeneous stationary state, homogeneous oscillations, spiking, and a stationary filament with increasing j_0 which is completely analogous to the experimentally observed behavior. Additionally, the functions $f(a,u)$ and $j(a,u)$ may look different for the p-n-p-n diode investigated experimentally. This may lead to a deformation of the phase diagram and may explain the different widths of the regimes, while the topological properties should be conserved. At the transition between the homogeneous oscillations and the periodic spiking the generic model exhibits chaotic behavior. This could be connected with the irregular oscillations observed experimentally at this transition point (Fig. 6).

In conclusion, we have shown that besides uniform relaxation oscillations, periodically spiking filaments may spontaneously appear in a semiconductor device. Our experimental results give clear indication that in a certain parameter range also irregularly spiking filaments with relatively quiescent phases of spatially uniform but temporally irregular oscillations occur close to the transition to stable uniform oscillations. As a further important result we point out that bistability between a spiking and a static filament causes hysteresis when the bias voltage source is swept up and down, respectively. This feature is a clear-cut distinction from the scenario of circuit limited oscillations which was proposed for the oscillations in p-Ge [4]. The trajectory of
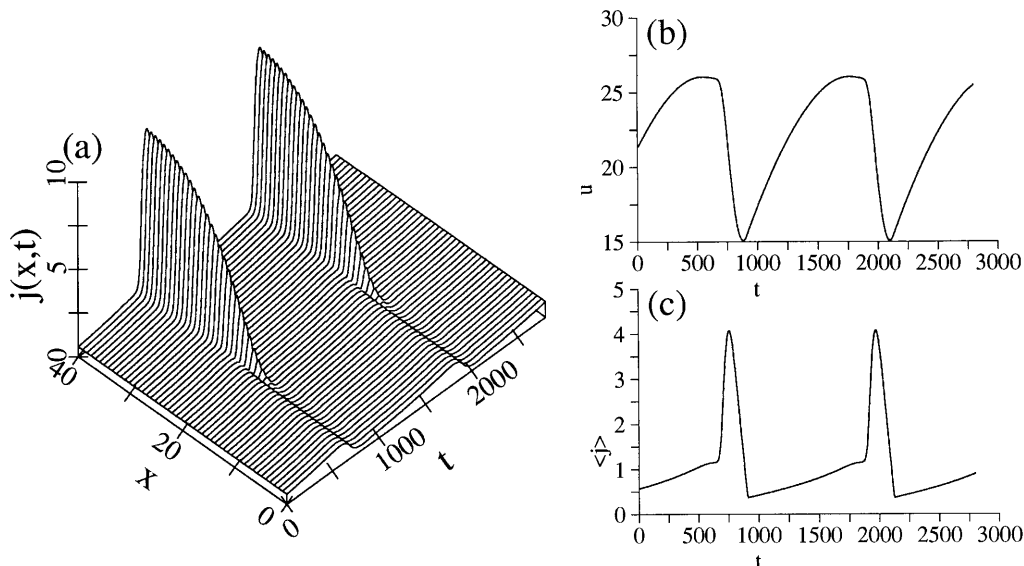
FIG. 10. Calculated current density $j(x,t)$ (a), voltage time signal $u(t)$ (b), and sample current time signal $\langle j \rangle(t)$ (c) of the periodic spiking for an inhomogeneous parameter $T(x) = T_0 + \Theta(x - l_x/2)\,\delta T - \Theta(l_x/2 - x)\,\delta T$ with $T_0 = 0.02$, $\delta T = 10^{-4} T_0 (\alpha = 0.03, j_0 = 1.1)$.

these relaxation-type oscillations runs through the filamentary branch and would stay there if the filament is stable. We emphasize that spiking oscillations in different semiconductor devices may also appear without any external capacitance. However, the possibility to vary an external capacitance provides a convenient method for a systematic analysis of various bifurcation scenarios of spiking filaments in semiconductor devices. All experimentally observed current-density patterns in the parameter range investigated can be consistently explained by a simple reaction-diffusion model.

[1] R. Symanczyk, S. Gaelings, and D. Jäger, Phys. Lett. A **160**, 397 (1991).

[2] R. Symanczyk, in *Nonlinear Dynamics and Pattern Formation in Semiconductors and Devices*, edited by F.-J. Niedernostheide, Springer Proceedings in Physics Vol. 79 (Springer, Berlin, 1995), pp. 200–219.

[3] F.-J. Niedernostheide, M. Arps, R. Dohmen, H. Willebrand, and H.-G. Purwins, Phys. Status Solidi B **172**, 249 (1992).

[4] U. Rau, W. Clauss, A. Kittel, M. Lehr, M. Bayerbach, J. Parisi, J. Peinke, and R. P. Huebener, Phys. Rev. B **43**, 2255 (1991).

[5] J. Spangler, U. Margull, and W. Prettl, Phys. Rev. B **45**, 12 137 (1992).

[6] K. M. Aliev, R. I. Bashirov, and M. M. Gadzhialiev, Fiz. Tekh. Poluprovodn. **28**, 899 (1994) [Sov. Phys. Semicond. **28**, 524 (1994)].

[7] R. Dohmen, thesis, University Münster, 1991 (unpublished).

[8] B. S. Kerner and V. V. Osipov, Zh. Éksp. Teor. Fiz. **83**, 2201 (1982) [Sov. Phys. JETP **56**, 1275 (1982)].

[9] B. S. Kerner and V. V. Osipov, Usp. Fiz. Nauk **157**, 201 (1989) [Sov. Phys. Usp. **32**, 101 (1989)].

[10] A. Wacker and E. Schöll, Semicond. Sci. Technol. **7**, 1456 (1992).

[11] A. Wacker and E. Schöll, Semicond. Sci. Technol. **9**, 592 (1994).

[12] A. Wacker and E. Schöll, Z. Phys. B **93**, 431 (1994).

[13] S. Bose, A. Wacker, and E. Schöll, Phys. Lett. A **195**, 144 (1994).

[14] F.-J. Niedernostheide, M. Ardes, M. Or-Guil, and H.-G. Purwins, Phys. Rev. B **49**, 7370 (1994).